JURNAL KIMIA VALENSI
p-ISSN: 2460-6065; e-ISSN: 2548-3013
Journal homepage: https://journal.uinjkt.ac.id/index.php/valensi
Research Article

Lanthanum Metal-Organic Frameworks as Binding Agent in Diffusive Gradients in Thin Films (DGT) for Phosphate Monitoring: Influence of pH and Competing Anions

Citra Santikasari [1,2], Asep Saefumillah[2]*, Agustino Zulys[2], Meyliana Wulandari[1]

[1]*Department of Chemistry, Faculty of Mathematics and Natural Science, Universitas Negeri Jakarta, Jakarta, 13220, Indonesia*
[2]*Department of Chemistry, Faculty of Mathematics and Natural Science, University of Indonesia, Depok, 16424, Indonesia*

Email: asep.saefumillah@sci.ui.ac.id

Article Info
Received: Feb 03, 2026
Revised: May 08, 2026
Accepted: May 10, 2026
Online: May 31, 2026

Citation:
Santikasari, C., Saefumillah, A., Zulys, A., Wulandari, M. (2026). Lanthanum Metal-Organic Frameworks as Binding Agent in Diffusive Gradients in Thin Films (DGT) for Phosphate Monitoring: Influence of pH and Competing Anions *Jurnal Kimia Valensi*, 12(1), 74-85.

Doi: 10.15408/jkv.v12i1.50201

Abstract
Phosphate mobility and bioavailability play critical roles in aquatic ecosystems, yet conventional monitoring methods are limited by sample disturbance and poor representation of in-situ conditions. The Diffusive Gradients in Thin Films (DGT) technique overcomes these limitations by enabling passive, in-situ measurement that accurately reflects natural solute diffusion and sediment resupply dynamics. This study introduces lanthanum metal-organic frameworks (La-MOF) as a novel selective binding agent in a DGT for in situ phosphate monitoring. La-MOF was synthesized via solvothermal using DMF (La-MOF 1) and mixed DMF/water (La-MOF 2), then characterized by XRD, FTIR, SEM-EDX, and BET analysis. Structural characterization confirmed successful framework formation for both materials. La-MOF 2 exhibited improved crystallinity, more homogeneous morphology, higher specific surface area (84.96 m^2 g^{-1}) and larger pore volume (0.090 cc g^{-1}) compared to La-MOF 1. The selectivity performance of La-MOF DGT was evaluated across pH 2-11 and in the presence of competing anions (NO_3^-, SO_4^{2-}, and CO_3^{2-}). Optimal phosphate uptake occurred at pH 4-7, corresponding to the predominance of $H_2PO_4^-$ species. The inhibitory effect on phosphate uptake followed the order: $NO_3^- > CO_3^{2-} > SO_4^{2-}$. These findings demonstrate the potential applicability of La-MOF as a selective binding agent for DGT-based phosphate monitoring in aquatic environments.

Keywords: DGT, lanthanum; MOF, phosphate

1. INTRODUCTION

The mobility and bioavailability of phosphate in aquatic and terrestrial environments have profound implications for nutrient cycling[1], eutrophication[2], and ecosystem health[3]. Accurate determination of bioavailable phosphate is essential for understanding phosphorus dynamics and supporting effective environmental monitoring and management. Conventional phosphate determination methods, including biological treatments[4], electrochemical and chemical precipitation[5], ion exchange[6], adsorption[7,8], crystallization[9], membrane filtration[10], and other analytical approaches, often suffer from limitations such as sample alteration, low temporal resolution, and the inability to reflect in situ conditions regarding solute resupply from solid phases[11]. These limitations become particularly important in dynamic aquatic systems where phosphate concentrations can continuously fluctuate due to adsorption-desorption equilibria, microbial activity, and physicochemical interactions.

To overcome these limitations, the Diffusive Gradients in Thin Films (DGT) technique has been widely applied as a passive sampling method capable of measuring labile and bioavailable species directly under in situ conditions[12]. Unlike conventional grab sampling methods, DGT enables time-integrated measurements that better reflect the dynamic exchange between dissolved species and surrounding solid phases[13]. Because the technique continuously removes labile analytes from solution through a binding layer, DGT can mimic natural uptake

processes occurring in biological systems, thereby providing a more environmentally relevant assessment of bioavailable nutrients and contaminants[14].

The DGT device consists of three main components: a filter membrane, a diffusive gel layer, and a binding layer[15]. During deployment, dissolved analytes diffuse through the filter membrane and diffusive gel before being immobilized by the binding layer, which ideally acts as an infinite sink[16]. This continuous uptake process establishes a stable concentration gradient across the diffusive layer, allowing analyte concentrations to be quantitatively determined based on Fick's first law of diffusion[17]. Under ideal conditions, the concentration measured by DGT reflects the labile and bioavailable fraction of analytes in the surrounding environment[15].

However, an increasing number of studies have reported limitations in DGT performance, particularly due to slow binding kinetics, insufficient adsorption capacity, and environmental matrix effects such as dissolved organic matter, ionic strength, ligand complexation, and diffusive boundary layers, all of which may disrupt steady-state diffusion conditions and bias DGT-derived concentrations[18-19]. Furthermore, when the binding layer capacity becomes saturated or when slowly dissociating complexes dominate, the binding layer no longer behaves as an infinite sink, and the linear uptake assumption may fail[20].

To overcome these limitations, recent research has explored nanostructured binding materials, particularly metal-organic frameworks (MOFs), as promising alternatives for the DGT binding layer due to their high surface area, tunable pore structure, and strong adsorption capability[21]. Among them, lanthanum-based metal-organic frameworks (La-MOF) have attracted attention because of their strong affinity towards phosphate species. Santikasari *et al*. (2020) demonstrated that La-MOF-based DGT systems exhibited enhanced phosphate uptake capacity (≈ 37.8 µg P in 24 h) compared to conventional binding layer [22].

Despite these advances, several critical aspects of La-MOF-based DGT performance remain insufficiently understood, including the influence of synthesis solvent composition on the structural and adsorption properties of the resulting frameworks, the effect of solution pH on phosphate speciation and uptake behavior, and the interference caused by competing anions such as nitrate (NO_3^-), carbonate (CO_3^{2-}), and sulfate (SO_4^{2-}).[23–25]. Addressing these aspects is essential for evaluating the practical applicability of La-MOF DGT systems under the variable physicochemical conditions commonly encountered in natural aquatic environments.

Therefore, this research extends previous La-MOF DGT research to provide a deeper understanding of phosphate adsorption behavior under varying environmental conditions. The specific objectives of this study were: (1) to compare the physicochemical properties of La-MOF synthesized solvothermally in DMF and mixed water/DMF solvent systems using XRD, FTIR, SEM-EDX, and BET analysis; (2) to evaluate the effect of solution pH (2–11) on phosphate accumulation by La-MOF DGT and determine the optimal pH range for phosphate uptake; and (3) to investigate the influence of competing anions such as nitrate (NO_3^-), carbonate (CO_3^{2-}), and sulfate (SO_4^{2-}) on phosphate accumulation and assess their competitive effects on La-MOF DGT performance.

2. RESEARCH METHODS

Materials

Materials used in this research were analytical grade and without any further purification step. $La(NO_3)_3.6(H_2O)$ by Sigma Aldrich, 1,4-benzenedicarboxylic acid (BDC) by Merck, acetone by Merck, N,N-dimethylformamide (DMF) by Sigma Aldrich, Acrylamide 40% by Sigma Aldrich, N,N' metylenebisacrilamide 1% by Merck, N,N,N',N'-tetramethylethylendiamine (TEMED) 99% by Merck, cellulose nitrate membrane filter by Whatman, KH_2PO_4 by Smartlab, NaOH by Merck, $NaNO_3$ by Merck, $NaHCO_3$ by Merck, Na_2SO_4 by Merck, HNO_3 by Merck, H_2SO_4 by Merck, $C_6H_8O_6$ by Merck, potassium antimony tartrate by Merck, ammonium heptamolybdate tetrahydrate by Merck, deionized water by Onemed.

Equipment

The equipment used in this research were standard laboratory glassware, magnetic stirrer, hot plate stirrer, teflon autoclave, thermometer, oven, pH meter, and filter paper. Meanwhile, material characterization was performed using Fourier Transform Infrared Spectroscopy (FTIR), X-Ray Powder Diffraction (XRD), Scanning Electron Microscopy – Energy Diffraction X-Ray Spectroscopy (SEM-EDX), UV-Visible Diffuse Reflectance Spectroscopy (UV-DRS), and Brunauer-Emmett Teller (BET) Surface Area Analyzer.

Synthesis and characterization of La-MOF

In this research, the synthesis of La-MOF was conducted using a solvothermal approach, which was adapted from the method reported by Liu *et al.* in 2016[26]. Specifically, 0.533 g $La(NO_3)_3.6(H_2O)$ and 0.514 g terephthalic acid (H_2BDC) were dissolved in 30 mL of N,N-dimethylformamide (DMF), then stirred for 30 minutes, later the product was known as La-MOF 1. For comparison, 0.437 g $La(NO_3)_3.6(H_2O)$ and 0.254 g BDC were dissolved in DMF/water solvent with a ratio of 20:1 v/v, then stirred for 30

minutes, and later the product was known as La-MOF 2. After 30 minutes, both mixtures were transferred to a teflon autoclave and heated at 120 °C for 20 hours. Then the products were washed repeatedly with acetone to remove unreacted ligands and residual solvents, then collected by filtration and dried at 60 °C for 24 hours.

The resulting La-MOF 1 and La-MOF 2 powders were characterized using X-Ray Diffraction (XRD) to confirm crystalline structure, Fourier Transform Infrared Spectroscopy (FTIR) to verify ligand coordination and functional groups, Scanning Electron Microscopy-Energy Dispersive X-Ray Spectroscopy (SEM-EDX) to analyze surface morphology and elemental composition, and BET Surface Area Analyzer to show that the addition of water in the solvent increased the surface area significantly, consistent with the previous findings by Santikasari *et al.* in 2020[22]. These characterization results confirmed that the solvothermal synthesis procedure was able to produced La-MOF with the expected structural features.

Synthesis of DGT Diffusive Layer

In this research, the membrane layer components required for assembling the DGT were were prepared using a polyacrylamide-based matrix. A stock gel solution was produced by mixing 40% acrylamide with 1% N, N'-methylenebisacrylamide (MBA) as the cross-linker, forming a homogeneous precursor that was suitable for both the diffusive and binding layers. The diffusive layer was synthesized by combining 10 mL of gel solution with 20 µL of N,N,N',N'- tetramethylethylendiamine (TEMED) as the polymerization accelerator and 70 µL of 10% ammonium persulfate as the initiator. This mixture was then cast into a glass mold and allowed to polymerize at 60 °C for 45 minutes to produce a mechanically stable diffusive layer.

Synthesis of Binding Layer with La-MOF as A Binding Agent

The preparation of the binding layer was prepared by following an identical polymerization procedure, with the addition of La-MOF powder dispersed evenly within the gel solution prior to polymerization to ensure uniform distribution of the binding agent throughout the polymer matrix. After curing, the binding layer was placed at the bottom of DGT mold, followed by the diffusive layer and a cellulose nitrate membrane positioned on top as the protective filter. The DGT cap was then tightened securely to ensure proper sealing, after which the assembled DGT was deployed in dissolved reactive phosphate (DRP) solution for concentration determination. The overall preparation methodology, including the incorporation of binding agent La-MOF into polyacrylamide matrix, follows the procedure described by Santikasari *et al.* in 2020[16], who developed a La-MOF-based binding agent for DGT applications.

Determination of Dissolved Reactive Phosphate (DRP) Using La-MOF DGT

The analytical procedure for determining dissolved reactive phosphate (DRP) accumulated in the DGT device was carried out using the ammonium molybdate spectrophotometric method, a well-established colorimetric technique commonly used for phosphate quantification in environmental samples[27]. After the deployment of the DGT device for 24 hours, the La-MOF binding layer was carefully removed from the DGT device and subjected to an elution process to release the accumulated phosphate into solution. The binding layer was immersed in 10 mL of HNO_3 for 24 hours to ensure complete desorption of phosphate from the La-MOF matrix. Prior to spectrophotometric analysis, the eluate was neutralized using 1 mol L^{-1} of NaOH in order to minimize interference caused by excess acidity.

The phosphate concentration in the eluate (C_e, $\mu g\ L^{-1}$) was determined using a Shimadzu UV-Vis Spectrophotometer 2450 at a wavelength of 720 nm, corresponding to the maximum absorbance wavelength of the molybdenum blue complex. The total mass of phosphate accumulated in the binding layer ($M, \mu g$) was calculated using equation (1)

$$M = C_e \times \left(V_{La-MOF} + V_{HNO_3} + V_{NaOH}\right)/f_e \qquad (1)$$

Where:

M = mass of phosphate accumulated in the binding layer (μg)

C_e = phosphate concentration in the eluate (µg L^{-1})

V_{La-MOF} = volume of La-MOF binding layer (2.7×10^{-4}L)

V_{HNO_3} = volume of HNO_3 eluent (0.01 L)

V_{NaOH} = volume of NaOH solution used for neutralization (L)

f_e = phosphate elution factor

The phosphate elution factor (f_e) was experimentally determined through phosphate recovery experiment using HNO_3 concentration ranging from 0.025 to 1 mol L^{-1}. Based on the recovery results, an elution factor value of 0.972 was obtained and subsequently applied in all DGT calculations. This procedure follows established DGT analytical protocols[12].

The phosphate concentration measured by the DGT (C_{DGT}) was calculated according to Fick's first law of diffusion using equation (2) :

$$C_{DGT} = \frac{M \times \Delta G}{D \times A \times t} \quad (2)$$

Where:

C_{DGT} = phosphate concentration measured by the DGT (μg L^{-1})

M = mass of phosphate accumulated in the binding layer (μg)

ΔG = total diffusive layer thickness consisting of the APA diffusive layer and cellulose nitrate membrane (0.123 cm)

D = diffusion coefficient of phosphate in the APA diffusive layer (2.2158×10^{-6} cm^2 s^{-1})

A = exposure area of the DGT device (3.14 cm^2)

t = deployment time (s)

The DGT device used in this study consisted of a standard piston-type DGT holder containing a cellulose nitrate membrane, an APA diffusive layer, and a La-MOF binding layer. All laboratory deployment experiments were conducted at room temperature (25 ± 1 °C). The diffusion coefficient (D) used in this research was experimentally determined under laboratory conditions following standard DGT procedures[17].

In addition, DGT performance validation was carried out through phosphate elution efficiency tests, diffusion coefficient determination, time-series uptake experiments, and concentration-dependent uptake experiments. A linear relationship between accumulated phosphate mass (mol L^{-1}) and deployment time (t) was obtained during the 24-hour deployment period, confirming that phosphate uptake followed the theoretical DGT diffusion model and that the binding layer behaved as an effective sink throughout the experiment[17].

To minimize the influence of the diffusive boundary layer (DBL), all laboratory experiments were performed under continuously stirred conditions to maintain stable hydrodynamic conditions around the DGT device. However, direct evaluation of DBL thickness using multiple diffusive layer thicknesses was not conducted in this research. Therefore, the influence of DBL should be considered when interpreting DGT-derived phosphate concentrations under low-flow environmental conditions.

Effect of pH and Interfering Anions on DRP Uptake in La-MOF-based DGT

To evaluate how chemical conditions affect phosphate uptake by the La-MOF DGT, the pH and interfering-ion variation test were carried out. In the pH variation test, the DGT units were placed in 250 mL of a 5 mg L^{-1} phosphate solution whose pH had been adjusted to values between 2 and 11 using HCl or NaOH. Each DGT unit was submerged to approximately three-quarters of the solution depth in the glass bottle, stirred for 24 hours, and then the phosphate bound to the La-MOF binding layer was eluted using 10 mL of the optimal HNO_3 eluent, neutralized with 1 mol L^{-1}. NaOH, and measured using the molybdenum blue method at 720 nm. The interfering-ion test followed the same procedure but included additional ions such as nitrate (NO_3^-), carbonate (CO_3^{2-}), and sulfate (SO_4^{2-}) added at 0.1, 0.2, and 0.3 mol L^{-1}. to the phosphate solution. After 24 hours of deployment, the accumulated phosphate was eluted and analysed in the same way. These tests were designed to evaluate how pH and common anions influence the performance of the La-MOF DGT.

3. RESULTS AND DISCUSSION

Characterization of La-MOF 1 and La-MOF 2 by XRD

Two types of lanthanum metal-organic frameworks (La-MOF) were synthesized using different solvent systems. La-MOF 1 refers to the material synthesized using DMF as the solvent, whereas La-MOF 2 refers to the material synthesized using a mixed DMF/water solvent system. Both La-MOF 1 and La-MOF 2 were obtained as shiny white powders. X-Ray Diffraction (XRD) analysis was conducted to evaluate the crystallinity and phase characteristics of the synthesized materials.

Figure 1a presents the XRD patterns of La-MOF 1 and La-MOF 2, while **Figure 1b** presents the comparison between La-MOF 1, La-MOF 2, and the reference diffraction pattern of lanthanum terephthalate tetrahydrate (JCPDS No. 00-034-1984). La-MOF 2, which was synthesized using DMF/water, exhibited higher crystallinity than La-MOF 1, which was synthesized in DMF. Higher crystallinity in MOF materials is often associated with improved structural order and can influence the surface area properties. When the diffraction patterns of La-MOF 1 and La-MOF 2 were compared with the JCPDS reference card 00-034-1984, both samples displayed a characteristic peak near 2 theta ≈ 9.55° for La-MOF 1 and 2 theta ≈ 9.54° for La-MOF 2, corresponding to the typical La-MOF structure reported by Liu *et al.* in 2016[26].

These peaks were slightly shifted to higher angles relative to the reference value (2 theta = 9.016°), which is consistent with a reduction in interplanar spacing (d-spacing) caused by compressive lattice strain[28]. Such shifts are commonly attributed to the presence of guest molecules within the MOF pores and to the breathing effect, where the framework undergoes slight structural contraction or expansion. The observed shift may also be influenced by residual 1,4-benzenedicarboxylic acid (BDC) that

did not fully coordinate with La^{3+} ions during synthesis. This interpretation is consistent with Liu *et al.* in 2016[17] who reported that the main peak around 2 theta = 9,5° correspond to a La-MOF structure closely related to the MIL-53 framework, and that deviations from the ideal MIL-53 peak position can occur due to unreacted ligands or remaining solvent molecules trapped within the pores [29].

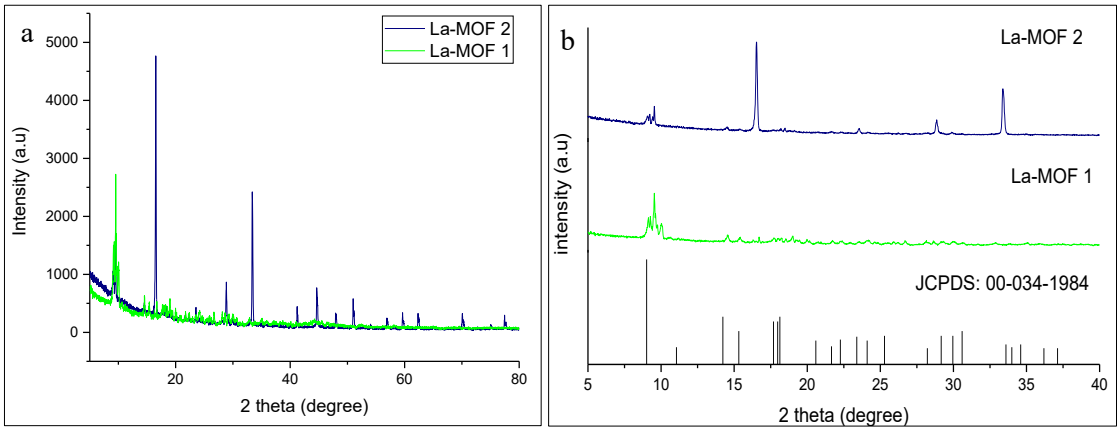

Figure 1. Characterization of La-MOF: (a) XRD pattern of La-MOF 1 and La-MOF 2; (b) comparison of XRD patterns with the reference pattern of lanthanum terephthalate tetrahydrate (JCPDS No. 00-034-1984).

Several differences in XRD peak intensity and secondary peak distribution were observed between La-MOF 1 and La-MOF 2, indicating that solvent composition significantly influenced crystal structure and framework ordering[30]. La-MOF 2 exhibited sharper and more intense diffraction peaks, suggesting a higher degree of crystallinity compared to La-MOF 1. This improvement can be attributed to the presence of a mixed DMF/water solvent system, which provided a more favorable environment for crystal growth during solvothermal synthesis[28]. In particular, water assisted the dissolution and ionization of the metal precursor, while DMF promoted gradual ligand deprotonation and controlled nucleation[31]. The synergistic effect of DMF and water facilitated more uniform coordination between La^{3+} ions and organic ligands, reduced rapid precipitation, and enhanced framework ordering. In contrast, the use of DMF alone in La-MOF 1 likely resulted in less controlled crystal growth and lower structural regularity. Consequently, La-MOF 2 showed better-defined diffraction peaks and higher relative crystallinity.

Characterization of La-MOF 1 and La-MOF 2 by FTIR

The FTIR spectra of La-MOF 1 and La-MOF 2 are presented in **Figure 2**. FTIR characterization is particularly valuable for MOF materials because it allows the identification of ligand coordination, functional groups, metal-ligand interactions, and the presence of residual solvent molecules. These features collectively provide insight into the chemical structure and successful formation of the framework.

As shown in **Figure 2**, La-MOF 1 and La-MOF 2 exhibited characteristic vibrational bands associated with the coordination between lanthanum ions and the organic linker BDC. The asymmetric and symmetric stretching modes of the carboxylate ($-COO^-$) groups appeared at 1563 cm^{-1} and 1397 cm^{-1}, respectively, for both La-MOF 1 and La-MOF 2. Importantly, the absence of the C=O stretching band at 1716 cm^{-1}, which is typical of free, uncoordinated BDC, confirmed that the carboxylate groups successfully coordinated to the lanthanum centers in both synthesized materials [22].

Additional peaks at 3059, 827, 675, and 753 cm^{-1} corresponded to the aromatic C-H stretching and bending vibrations of the benzene ring in BDC, and these features appeared consistently in both La-MOF 1 and La-MOF 2, further supporting the incorporation of the linker into the MOF structure[32,33]. Both spectra also display vibrational bands at 2937 cm^{-1} and 1660 cm^{-1}, attributed to the asymmetric stretching of methyl groups and the C=O vibration from residual DMF molecules[34]. The presence of these bands suggested that a small amount of DMF remained trapped within the pores, which is common for solvothermal synthesis of MOF materials. Altogether, the FTIR results confirmed that coordination between La^{3+} ions and BDC ligand occurred successfully in both La-MOF 1 and La-MOF 2, while minor differences in peak intensity may reflect variations in crystallinity and residual solvent content between the two samples.

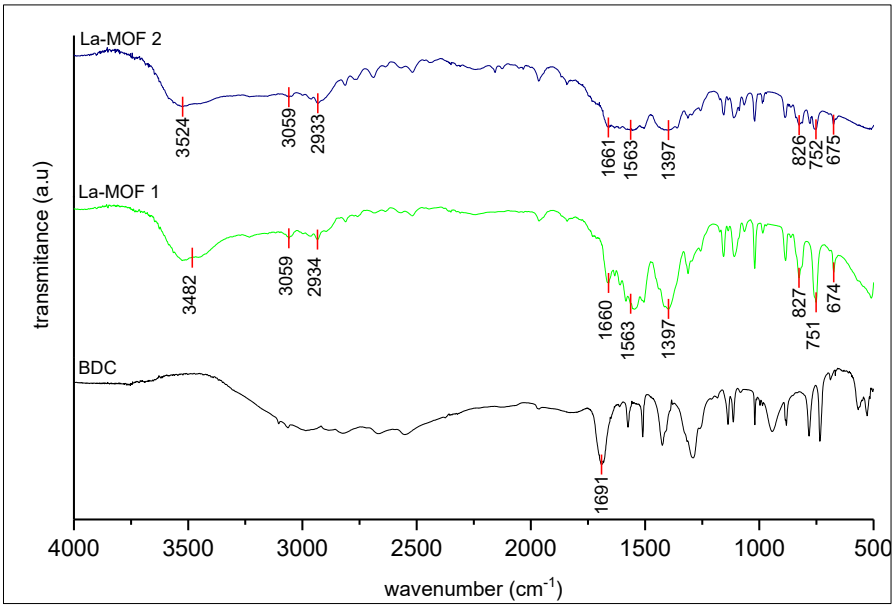

Figure 2. FTIR pattern of BDC, La-MOF 1[22], and La-MOF 2

Characterization of La-MOF 1 and La-MOF 2 by SEM-EDX

The morphology and elemental distribution of La-MOF 1 and La-MOF 2 were observed by Scanning Electron Microscopy (SEM) and Energy Dispersive X-ray Spectroscopy (EDX), as shown in **Figure 3**. The SEM images were captured at 10,000× magnification, where Figure 3a corresponds to La-MOF 1 and Figure 3b corresponds to La-MOF 2. At this magnification, most particles of La-MOF 1 appeared in aggregate and exhibited a somewhat irregular needle-like shape, suggesting less uniform crystal growth. In contrast, La-MOF 2, which was synthesized using water/DMF, showed a more well-defined needle-like morphology with improved uniformity and particle regularity. These morphological differences indicated that solvent composition influenced the nucleation and crystal growth process during synthesis. La-MOF 2 with DMF/water solvent system likely promoted slower and more controlled crystal growth, resulting in improved structural ordering and higher crystallinity, which is consistent with the XRD results discussed previously.

These visual differences indicated that the framework quality of La-MOF 2 is superior to that of La-MOF 1, likely due to the influence of solvent choice on nucleation and crystal growth during synthesis. EDX analysis further confirmed the elemental composition of both samples, verifying the presence of lanthanum (La), carbon (C), and oxygen (O) consistent with the designed MOF framework. As shown in **Table 1**, these elements represent the main constituents of the La-MOF framework. Hydrogen atoms originating from the BDC linker could not be detected by EDX due to their very low atomic mass and the inherent limitation of EDX analysis in detecting light elements. Therefore, the elemental composition discussion was focused on lanthanum (La), carbon (C), and oxygen (O).

Table 1 showed that La-MOF 2 contained a substantially higher proportion of La (13.83%) and O (53.70%) than La-MOF 1 (3.10% La and 22.26% O). This compositional shift strongly suggested that La-MOF 2 possessed a more extensive network of La-O coordination bonds, involving oxygen atoms from both the BDC ligands and residual water molecules. The higher La and O contents observed in La-MOF 2 suggested a more complete coordination interaction between La^{3+} ions and carboxylate groups from the BDC ligands, leading to the formation of a more structurally ordered framework. In addition, the improved needle-like morphology observed in the SEM images may contributed to a greater surface area and potentially enhanced phosphate adsorption performance.

In contrast, the relatively lower La and O percentages in La-MOF 1 may indicate incomplete framework formation or the presence of residual uncoordinated organic ligands. This observation is also consistent with the broader diffraction peaks observed in the XRD analysis, which suggested lower crystallinity for La-MOF 1. Therefore, the combined SEM-EDX and XRD results indicated that the mixed DMF/water solvent system produced La-MOF material with improved morphology, crystallinity, and structural integrity compared with synthesis in DMF.

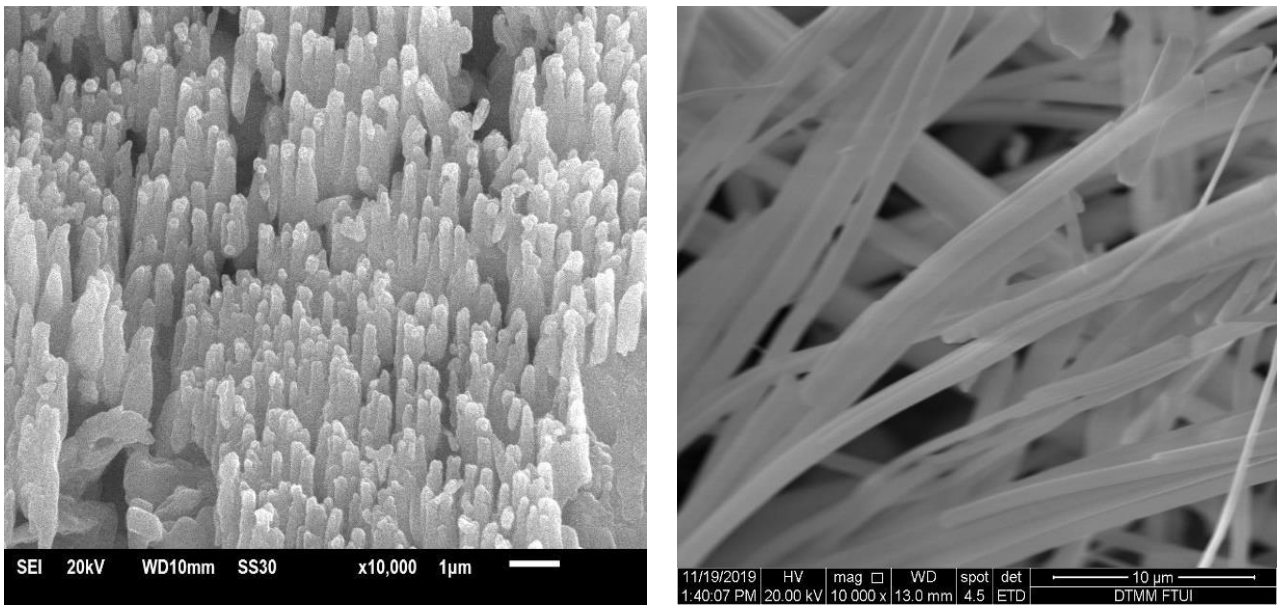

a. La-MOF 1 b. La-MOF 2

Figure 3. SEM images of La-MOF 1 (a) and La-MOF 2 (b) in 10,000× magnification

Table 1. Elemental composition of La-MOF 1 and La-MOF 2 by EDX

Percent of Element	La-MOF 1	La-MOF 2
La	3.10	13.83
C	74.24	32.46
O	22.66	53.70

Pore Volume and Surface Area Characterization of La-MOF 1 and La-MOF 2 by BET

The specific surface area of La-MOF 2 have been previously reported by Santikasari *et al.* [22], whereas the present research provides additional characterization data related to the surface area of La-MOF 1 and pore volume for both La-MOF 1 and La-MOF 2 in order to further evaluate the properties of La-MOF 1 and La-MOF 2. As showed in **Table 2**, La-MOF 2 exhibited a higher specific surface area and pore volume compared with La-MOF 1. These results indicated that the mixed DMF/water solvent system in La-MOF 2 significantly enhanced the porosity and surface development of the synthesized La-MOF material.

The enhanced surface area and pore volume observed in La-MOF 2 may be attributed to the roles of water and DMF during solvothermal synthesis. The presence of water in a mixed solvent system can influence the hydrolysis process and coordination interaction between La^{3+} ions and BDC ligands, thereby promoting more controlled nucleation and crystal growth [35–37]. As a result, La-MOF 2 formed a more open and porous framework structure with improved structural ordering. This interpretation is consistent with the SEM results, which showed that La-MOF 2 exhibited a more homogeneous needle-like morphology, as well as with the XRD results showing higher crystallinity compared with La-MOF 1.

Table 2. Pore volume and surface area of La-MOF 1 and La-MOF 2

MOF	Pore volume (cc/g)	Surface Area (m^2/g)
La-MOF 1	0.012	7.939
La-MOF 2	0.090	84.957

Similar effects of mixed-solvent systems on MOF porosity have been reported in several recent studies, in which controlled water addition acted as a modulator, enhancing crystal growth, pore formation, and structural stability[38–40]. Based on these improvements, La-MOF 2 was selected as the optimized material for incorporation into the DGT binding layer, as its higher surface area and porosity are advantageous for enhancing phosphate uptake capacity and diffusion-limited performance.

Effect of solution pH on phosphate removal by La-MOF DGT

Orthophosphate in aqueous systems exists as multiple species such as H_3PO_4, $H_2PO_4^-$, HPO_4^{2-}, and PO_4^{3-}, whose distribution is strongly governed by the pH of the solution[41]. As showed in **Figure 4**, phosphate speciation changes systematically with increasing pH due to stepwise deprotonation of phosphoric acid. Under very acidic conditions (pH < 2), phosphate predominantly exists as neutral phosphoric acid (H_3PO_4). As the pH increases to

approximately pH 2-7, the first dissociation of phosphoric acid occurs, resulting in the formation of dihydrogen phosphate ($H_2PO_4^-$), which becomes the dominant phosphate species within this pH range. Near neutral pH, particularly around pH 6-7, both $H_2PO_4^-$ and HPO_4^{2-} coexist in significant proportions due to the second dissociation equilibrium. Under more alkaline conditions, around pH 7-12, HPO_4^{2-} gradually becomes the predominant phosphate species. Under strongly alkaline conditions (pH > 12), phosphate mainly exists as phosphate ions (PO_4^{3-}) following further deprotonation [41].

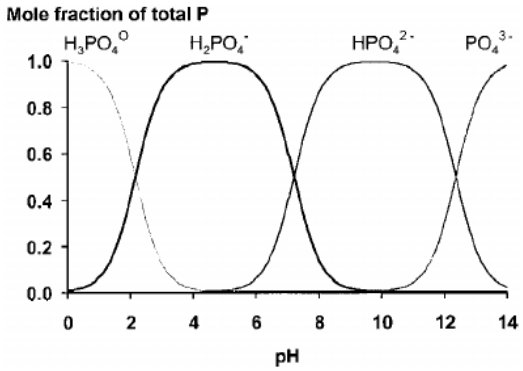

Figure. 4 Phospate speciation at any pH[42]

The transition among phosphate species significantly influences phosphate behavior in aqueous systems because each species possesses different charges, protonation states, and interaction capabilities toward adsorption sites. Changes in phosphate speciation may therefore alter the affinity of phosphate toward the La-MOF binding layer, ultimately affecting phosphate accumulation within the DGT system. In addition, pH not only controls phosphate speciation but also influences the surface charge of the La-MOF binding layer and the interaction between phosphate species and the active adsorption sites of the binding agent. Consequently, phosphate uptake by La-MOF DGT strongly depends on the prevailing phosphate species under specific pH conditions, making evaluation of pH effects essential for understanding the adsorption performance of the La-MOF-based DGT system.

To investigate this effect, phosphate solutions were adjusted to pH values ranging from 2 to 11 using HCl and NaOH. The La-MOF DGT devices were then deployed in 250 mL phosphate solution (5 mg L^{-1}) for 24 h, after which phosphate uptake was evaluated using the $C_{DGT}/C_{Initial}$ ratio. A ratio greater than 1 indicates that the amount of orthophosphate accumulated by the DGT binding layer exceeded the amount expected from the initial solution concentration, reflecting efficient phosphate uptake under the corresponding pH condition[43].

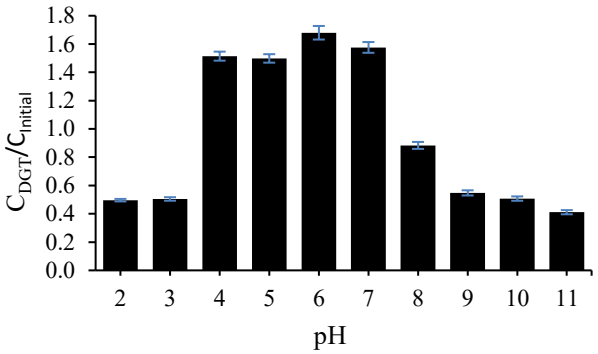

Figure. 5 Effect of pH on DRP uptake of La-MOF DGT

Figure 5 Illustrated the relationship between solution pH (x-axis) and the phosphate uptake efficiency, expressed as $C_{DGT}/C_{Initial}$ (y-axis). The results showed that the La-MOF DGT exhibits selective affinity for $H_2PO_4^-$, consistent with the higher uptake across pH 4-7. This observation aligns with established speciation chemistry in **Figure 4**, where $H_2PO_4^-$ dominates under mildly acidic to neutral conditions[42]. Moreover, changes in solution pH before and after deployment were negligible, indicating that the uptake mechanism is unlikely to be dominated by electrostatic binding, which typically alters solution pH through release or consumption. Instead, the findings suggest that the mechanism involves physical adsorption and ligand-exchange interactions between phosphate and La-MOF functional sites. Similar pH-dependent adsorption trends have been reported for phosphate removal using other MOF and adsorbent systems, where maximum adsorption occurs under conditions where $H_2PO_4^-$ is the dominant species. For example, in La@ZIF-8 composites, the adsorption capacity peaked around neutral pH values, which was attributed to dominant $H_2PO_4^-$ interactions, whereas adsorption declined under acidic or alkaline conditions due to changes in speciation and surface charge effects[44].

At pH values above 7, the uptake ratio declined sharply as $H_2PO_4^{-2}$ and PO_4^{3-} became more abundant. These higher-valent phosphate species are less effectively captured by La-MOF binding sites, mostly due to changes in both electrostatic interactions and steric effects that diminish favorable adsorption. This trend is consistent with general phosphate adsorption behavior, where species with higher negative charge (such as $H_2PO_4^{2-}$ and PO_4^{3-}) are often less efficiently adsorbed unless specific inner-sphere complexation mechanisms dominate[45].

Changes in solution pH before and after deployment were minimal, suggesting that electrostatic binding alone is not the primary mechanism governing phosphate uptake in DGT systems. If electrostatic attraction between La^{3+} and

PO_4^{3-} were dominant, one would expect higher uptake at high pH values where PO_4^{3-} prevalence increases. Instead, the observed decline in uptake at elevated pH indicates that ligand exchange and physical adsorption interactions, particularly with the $H_2PO_4^-$ species, are more critical for effective binding in the La-MOF DGT. These results align with literature describing pH-dependent adsorption mechanisms in MOF and other adsorbents, where ligand exchange and inner-sphere complexation often control performance across pH ranges[26,46].

Altogether, these findings demonstrate that La-MOF DGT exhibits selective affinity for $H_2PO_4^-$, with optimal uptake under mildly acidic to neutral pH conditions (4-7), which is consistent with phosphate speciation behavior. This pH-dependent uptake profile has important implications for environmental monitoring, highlighting the need to consider solution pH and dominant phosphate species when interpreting DGT measurements in complex water matrices.

Effect of anion interferences in solution on phosphate removal by La-MOF DGT

The influence of coexisting anions on orthophosphate uptake by the La-MOF DGT system was evaluated using three commonly occurring anions in natural waters, such as nitrate (NO_3^-), carbonate (CO_3^{2-}), and sulfate (SO_4^{2-})[26]. These anions are known to compete with phosphate for adsorption sites in metal-based adsorbents and can cause significant measurement bias in DGT-based phosphate assessments. To systematically investigate this effect, each interfering ion was added to 250 mL of 5 ppm phosphate solution at increasing concentration from 0.1 to 0.3 mol L^{-1}. The resulting phosphate uptake was expressed as the ratio $C_{DGT}/C_{Initial}$, where a value greater than 1 indicates enhanced uptake relative to the initial concentration, and values below 1 indicate inhibition.

Figure 6 illustrates the relationship between interfering ion concentration (x-axis) and the phosphate uptake efficiency, expressed as $C_{DGT}/C_{Initial}$ (y-axis). As the concentration of interfering ions increases, shifts in phosphate uptake become apparent, allowing their competitive behavior to be compared directly. A clear trend emerged in the presence of nitrate (NO_3^-), even at the lowest concentration tested (0.1 mol L^{-1}), NO_3^- caused a sharp decrease in $C_{DGT}/C_{Initial}$ to approximately 0.6, indicating strong suppression of phosphate accumulation by La-MOF. Notably, further increases in nitrate concentration did not produce substantial additional inhibition, suggesting that NO_3^- effectively saturates competitive binding at a low concentration. In contrast, carbonate (CO_3^{2-}) and sulfate (SO_4^{2-}) showed a more gradual, concentration-dependent decrease in $C_{DGT}/C_{Initial}$, as their concentration increases from 0.1 M to 0.3 M, phosphate uptake is progressively inhibited, although the magnitude of the effect remains lower than that of nitrate (NO_3^-) at equivalent concentrations.

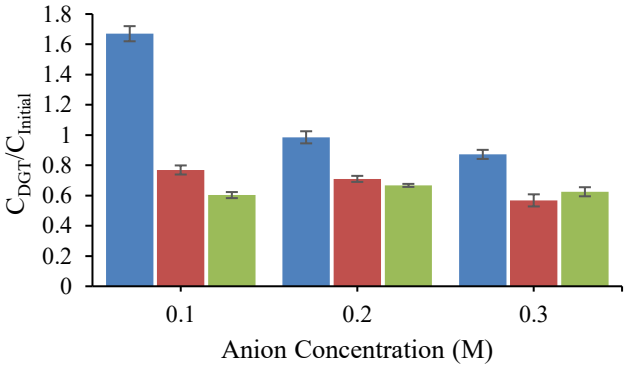

Figure 6. Effects of anion interferences on DRP uptake of La-MOF DGT

Although carbonate (CO_3^{2-}) is theoretically expected to exhibit a strong affinity toward La^{3+} sites based on Hard and Soft Acid-Base (HSAB) interactions, the research results showed that nitrate (NO_3^-) caused greater inhibition under the investigated conditions. This observation differs from several previous studies on lanthanum-based phosphate adsorbents, where carbonate (CO_3^{2-}) has often been reported as a stronger competing ion due to its high affinity toward lanthanum active sites [23–25]. Therefore, the competitive behavior observed in the present study may not be governed solely by thermodynamic adsorption affinity.

One possible explanation is that diffusion and transport processes within the DGT configuration also contributed to the observed uptake behavior. Nitrate ions (NO_3^-) possessed smaller hydrated radii and higher mobility in aqueous solution compared with carbonate (CO_3^{2-}) and sulfate (SO_4^{2-}) ions, which may facilitate faster diffusion through the diffusive layer and more rapid occupation of accessible adsorption regions near the La-MOF surface [17]. In contrast, carbonate (CO_3^{2-}) and sulfate (SO_4^{2-}) ions may diffuse more slowly due to their larger hydrated structures and stronger hydration shells, potentially limiting their diffusion rates within the DGT system. However, this interpretation remains speculative because diffusion kinetics and ion transport behavior were not directly evaluated in this research. Therefore, additional investigations involving kinetic adsorption studies of diffusion controlled transport experiments are necessary to clarify the dominant mechanism responsible for anion interference in the La-MOF DGT.

Interestingly, at 0.1 mol L^{-1} sulfate (SO_4^{2-}), the $C_{DGT}/C_{Initial}$ value reached up to 1.48, suggesting that sulfate (SO_4^{2-}) produced only limited interference under low-concentration conditions. However,

increasing sulfate concentration gradually reduced phosphate uptake efficiency, indicating increasing competition for adsorption sites. Overall, the competitive effect observed in this study followed the order: nitrate (NO_3^-) > carbonate (CO_3^{2-}) > sulfate (SO_4^{2-}). These results suggest that phosphate uptake in the La-MOF DGT is influenced not only by thermodynamic adsorption affinity but also by ion mobility.

Comparable trends have been reported in earlier work using ferrihydrite-based DGT by Maimulyanti *et al.* in 2018, [47], where nitrate caused the most significant reduction in phosphate accumulation, followed by sulfate and carbonate. This reinforces the interpretation that diffusion-driven competition may play an important role in DGT systems beyond thermodynamic considerations alone. Overall, the results demonstrate that interfering anions can substantially affect the performance of La-MOF DGT, with nitrate exhibiting the strongest inhibitory effect even at low concentrations. Therefore, the competitive behavior of these anions should be carefully considered when applying La-MOF DGT for phosphate monitoring in waters containing high levels of nitrate (NO_3^-), carbonate (CO_3^{2-}), or sulfate (SO_4^{2-}).

4. CONCLUSIONS

In this research, La-MOF synthesized using a mixed DMF/water solvent system (La-MOF 2) exhibited higher surface area, larger pore volume, and improved crystallinity compared to La-MOF synthesized using DMF (La-MOF 1), indicating that solvent composition significantly influenced the physicochemical properties of La-MOF. La-MOF 2 was then applied as the binding agent for binding layer of DGT system for in situ phosphate adsorption. Evaluation of the pH effect showed that phosphate uptake by the La-MOF DGT system strongly depended on solution pH, with optimum uptake observed at pH 4-7, particularly around pH 6, corresponding to the predominance of $H_2PO_4^-$ species. In addition, the presence of competing anions influenced phosphate accumulation. The competitive effect followed the order: nitrate (NO_3^-) > carbonate (CO_3^{2-}) > sulfate (SO_4^{-2}) under the experimental conditions investigated. Overall, these results demonstrate the potential applicability of La-MOF DGT for phosphate monitoring in aquatic environments under varying chemical conditions.

REFERENCES

1. Guignard MS, Leitch AR, Acquisti C, Eizaguirre C, Elser JJ, Hessen DO, Jeyasingh PD, Neiman M, Richardson AE, Soltis PS, Soltis DE, Stevens CJ, Trimmer M, Weider LJ, Woodward G and Leitch.Impacts of nitrogen and phosphorus: From genomes to natural ecosystems and agriculture. *Front Ecol Evol*. 2017;5(7):258706. doi:10.3389/FEVO.2017.00070
2. Wurtsbaugh WA, Paerl HW, Dodds WK. Nutrients, eutrophication and harmful algal blooms along the freshwater to marine continuum. *Wiley Interdisciplinary Reviews: Water*. 2019;6(5):e1373. doi:10.1002/WAT2.1373
3. Rönspieß L, Nausch G, Schulz-Bull D. Bioavailability of various phosphorus fractions and their seasonality in a eutrophic estuary in the southern baltic sea – a Laboratory approach. *Front Mar Sci*. 2021;8:715238. doi:10.3389/FMARS.2021.715238
4. Klein K, Mandel A, Lilleoja H, Salmar S, Tenno T. Assessment of enhanced biological phosphorus removal process inhibition. *SN Appl Sci*. 2020;2(9):1-10. doi:10.1007/S42452-020-03281-1
5. Rajaniemi K, Hu T, Nurmesniemi ET, Tuomikoski S, Lassi U. Phosphate and ammonium removal from water through electrochemical and chemical precipitation of struvite. *Processes*. 2021;9(1):1-13. doi:10.3390/pr9010150
6. Guida S, Rubertelli G, Jefferson B, Soares A. Demonstration of ion exchange technology for phosphorus removal and recovery from municipal wastewater. *Chemical Engineering Journal*. 2021;420:129913. doi:10.1016/J.CEJ.2021.129913
7. Vikrant K, Kim KH, Ok YS. Engineered/designer biochar for the removal of phosphate in water and wastewater. *Science of The Total Environment*. 2018;616-617:1242-1260. doi:10.1016/J.SCITOTENV.2017.10.193
8. Sun J, Gao A, Wang X, Xu X, Song J. Removal of phosphorus from wastewater by different morphological alumina. *Molecules 2020, Vol 25, Page 3092*. 2020;25(13):3092. doi:10.3390/MOLECULES25133092
9. Hiroyuki H, Katsutoshi I, Hiroyuki H, Katsutoshi I. Phosphorus recovery by crystallization. *Phosphorus - Recovery and Recycling*. 2018. doi:10.5772/INTECHOPEN.81549
10. Smol M. The use of membrane processes for the removal of phosphorus from wastewater. *Desalination Water Treat*. 2018;128:397-406. doi:10.5004/DWT.2018.23105
11. Rathnayake KN, Bennett WW, Teasdale PR, Huang J, Welsh DT. Comparing in situ colorimetric DET and DGT techniques with ex situ core slicing and centrifugation for measuring ferrous iron and dissolved sulfide in

coastal sediment pore waters. *Chemosphere*. 2017;188:119-129. doi:10.1016/j.chemosphere.2017.08.144

12. Puschenreiter M. William D. Diffusive gradients in thin-films for environmental measurements. *Analytical and Bioanalytical Chemistry 2017 409:8*. 2017;409(8):1973-1974. doi:10.1007/S00216-016-0178-5
13. Liu H, Chi L, Shen J, Arandiyan H, Wang Y, Wang X. Principles, applications, and limitations of diffusive gradients in thin films induced fluxed in soils and sediments. *Chemosphere*. 2024;350. doi:10.1016/J.CHEMOSPHERE.2023.141061
14. Senila M, Kovacs E. Use of diffusive gradients in thin-film technique to predict the mobility and transfer of nutrients and toxic elements from agricultural soil to crops—an overview of recent studies. *Environmental Science and Pollution Research*. 2024;31(24):34817-34838. doi:10.1007/S11356-024-33602-5/TABLES/2
15. Cao H, Bu Q, Li Q. Development and applications of diffusive gradients in thin films for monitoring pharmaceuticals in surface waters. *Environmental Pollution*. 2022;311:119979. doi:10.1016/J.ENVPOL.2022.119979
16. Zhu Q, Ji J, Tang X, Wang C, Sun H. Bioavailability assessment of heavy metals and organic pollutants in water and soil using DGT: A Review. *Applied Sciences 2023, Vol 13, Page 9760*. 2023;13(17):9760. doi:10.3390/APP13179760
17. Davison W, Zhang H. In situ speciation measurements of trace components in natural waters using thin-film gels. *Nature 1994 367:6463*. 1994;367(6463):546-548. doi:10.1038/367546a0
18. Liu H, Chi L, Shen J, Arandiyan H, Wang Y, Wang X. Principles, applications, and limitations of diffusive gradients in thin films induced fluxed in soils and sediments. *Chemosphere*. 2024;350.doi:10.1016/j.chemosphere.2023.141061
19. Xu X, Peck E, Fletcher DE, Korotasz A, Perry J. Limitations of applying diffusive gradients in thin films to predict bioavailability of metal mixtures in aquatic systems with unstable water Chemistries. *Environ Toxicol Chem*. 2020;39(12):2485-2495. doi:10.1002/ETC.4860
20. Sans-Duñó J, Cecilia J, Galceran J, Puy J, Baeyens W, Gao Y. Back accumulation of diffusive gradients in thin-films devices with a stack of resin discs to assess availability of metal cations to biota in natural waters. *Environ Sci Technol*. 2023;57(20):7840-7848. doi:10.1021/ACS.EST.3C00799
21. Chavan GT, Kim H, Shim KY. Innovative binding gels in diffusive gradients in thin film to detect hazardous contaminants: A critical review. *Journal of Hazardous Materials Advances*. 2025;17:100530. doi:10.1016/J.HAZADV.2024.100530
22. Santikasari C, Saefumillah A, Zulys A. Lanthanum based metal organic frameworks as a new binding agent material for diffusive gradient in thin film (DGT) technique in bioavailability of phosphate removal. *IOP Conf Ser Mater Sci Eng*. 2020;902(1). doi:10.1088/1757-899X/902/1/012043
23. Pincus LN, Rudel HE, Petrović P V. Exploring the mechanisms of selectivity for environmentally significant oxo-anion removal during water treatment: A Review of Common Competing Oxo-Anions and Tools for Quantifying Selective Adsorption. *Environ Sci Technol*. 2020;54(16):9769-9790. doi:10.1021/ACS.EST.0C01666
24. Alam MM, Srinivasan V, Mueller A V., Gu AZ. Status and advances in technologies for phosphorus species detection and characterization in natural environment- A comprehensive review. *Talanta*. 2021;233:122458. doi:10.1016/J.TALANTA.2021.122458
25. Zhang S, Xie F, Tang Z, Zhao T, Fang M, Giesy JP. Adsorption of phosphate by surface precipitation on lanthanum carbonate through in situ anion substitution reactions. *Front Environ Sci*. 2022;10:858258. doi:10.3389/FENVS.2022.858258/TEXT
26. Liu H, Guo W, Liu Z, Li X, Wang R. Effective adsorption of phosphate from aqueous solution by La-based metal-organic frameworks. *RSC Adv*. 2016;6(107):105282-105287. doi:10.1039/C6RA24568D
27. Warwick C, Guerreiro A, Soares A. Sensing and analysis of soluble phosphates in environmental samples: A review. *Biosens Bioelectron*. 2013;41(1):1-11. doi:10.1016/J.BIOS.2012.07.012
28. Akhundzadeh Tezerjani A, Halladj R, Askari S. Different view of solvent effect on the synthesis methods of zeolitic imidazolate framework-8 to tuning the crystal structure and properties. *RSC Adv*. 2021;11(32):19914-19923. doi:10.1039/D1RA02856A
29. Cheng X, Zhang A, Hou K, et al. Size- and morphology-controlled NH2-MIL-53(Al) prepared in DMF-water mixed solvents. *Dalton Transactions*. 2013;42(37):13698-13705. doi:10.1039/C3DT51322J

30. Seetharaj R, Vandana PV, Arya P, et al. Dependence of solvents, pH, molar ratio and temperature in tuning metal organic framework architecture. *Arabian Journal of Chemistry*. 2019;12(3):295-315. doi:10.1016/J.ARABJC.2016.01.003
31. Carpenter BP, Talosig AR, Rose B, Di Palma G, Patterson JP. Understanding and controlling the nucleation and growth of metal–organic frameworks. *Chem Soc Rev*. 2023;52(20):6918-6937. doi:10.1039/D3CS00312D
32. Safinejad M, Rigi A, Zeraati M. Lanthanum-based metal organic framework (La-MOF) use of 3,4-dihydroxycinnamic acid as drug delivery system linkers in human breast cancer therapy. *BMC Chemistry 2022 16:1*. 2022;16(1):93-. doi:10.1186/S13065-022-00886-Y
33. Elenkova D, Dimitrova Y, Tsvetkov M. Investigation of the sensing properties of Lanthanoid Metal–Organic Frameworks (Ln-MOFs) with terephthalic acid. *Molecules*. 2024;29(15):3713. doi:10.3390/MOLECULES29153713/S1
34. Hadjiivanov KI, Panayotov DA, Mihaylov MY. Power of infrared and raman spectroscopies to characterize Metal-Organic Frameworks and investigate their interaction with guest molecules. *Chem Rev*. 2020;121(3):1286-1424. doi:10.1021/ACS.CHEMREV.0C00487
35. Shamsulazri NAN, Saifullizan N, Sabar S. Recent progress of mixed-linker Zn2+ metal-organic frameworks and their applications. *Polyhedron*. 2025;282:117808. doi:10.1016/J.POLY.2025.117808
36. Soni S, Bajpai PK, Arora C. A review on metal-organic framework: Synthesis, properties and ap-plication. *Characterization and Application of Nanomaterials*. 2020;3(2):87-106. doi:10.24294/CAN.V3I2.551
37. Alnafisah MS, Alharbi KN, Almuqati NS. Effect of solvent selection on Zn-MOFs synthesized for hydrogen storage applications. *Int J Hydrogen Energy*. 2025;120:393-402. doi:10.1016/J.IJHYDENE.2025.03.326
38. Liu X, Wang X, Kapteijn F. Water and Metal–Organic Frameworks: From Interaction toward Utilization. *Chem Rev*. 2020;120(16):8303-8377. doi:10.1021/ACS.CHEMREV.9B00746
39. Sun J, Yu X, Zhao S, Chen H, Tao K, Han L. Solvent-controlled morphology of amino-functionalized bimetal Metal–Organic Frameworks for asymmetric supercapacitors. *Inorg Chem*. 2020;59(16):11385-11395. doi:10.1021/ACS.INORGCHEM.0C01157
40. Wang C, Li H, Xue J. Lanthanide-based MOFs with metal-node-modulated energy transfer for multifunctional X-ray imaging platforms. *Chemical Engineering Journal*. 2025;526:171125. doi:10.1016/J.CEJ.2025.171125
41. Spivakov BYA, Maryutina TA, Muntau H. Phosphorus speciation in water and sediments (Technical Report). *Pure and Applied Chemistry*. 1999;71(11):2161-2176. doi:10.1351/PAC199971112161/PDF
42. Hinsinger P. Bioavailability of soil inorganic P in the rhizosphere as affected by root-induced chemical changes: A review. *Plant Soil*. 2001;237(2):173-195. doi:10.1023/A:1013351617532/METRICS
43. Saefumillah A, Rahmaniarti RH. Pengembangan metode DGT (Diffusive Gradient In Thin Film) dengan binding gel Fe-Al-Oksida dan pengikat silang N,N'-methylenebisacrylamide untuk penyerapan fosfat dalam air. *Jurnal Kimia Valensi*. 2015;1(1):20-25. doi:10.15408/JKV.V0I0.3597
44. Li J, Chang H, Li Y, et al. Synthesis and adsorption performance of La@ZIF-8 composite metal–organic frameworks. *RSC Adv*. 2020;10(6):3380-3390. doi:10.1039/C9RA10548D
45. Nadagouda MN, Varshney G, Varshney V, Hejase CA. Recent advances in technologies for phosphate removal and recovery: A Review. *ACS Environmental Au*. 2024;4(6):271-291. doi:10.1021/ACSENVIRONAU.3C00069
46. Zhou Z, Li D, Huang W. Phosphate adsorption on cerium/terephthalic acid Metal–Organic Frameworks (Ce-MOF) driven by effective electrostatic attraction and ligand exchange in a wide pH range. *Chem Asian J*. 2023;18(11):e202300202. doi:10.1002/ASIA.202300202
47. Maimulyanti A, Saefumillah A, Suseno H. Effect of ph and anion interferences on determination of orthophosphate speciation by Diffusive Gradient in Thin Film (DGT) technique. *Rasayan J Chem*. 11(3):1222-1228. doi:10.31788/RJC.2018.113305